Modelling of Fragile Coal Mine Roof and Estimation of Rock Loads—Some Empirical and Numerical Methods

Avinash Paul[1] · V. M. S. R. Murthy[2] · Amar Prakash[1] · Ajoy Kumar Singh[1] · John Loui Porathur[1]

Abstract

Weak, layered, and fragile rock mass formation, if not supported properly, is subject to roof failure thereby affecting safety and productivity in underground coal mines. Though Central Mining Research Institute – Indian School of Mines Rock Mass Rating (CMRI-ISM RMR) based well-defined support design guidelines are established, still occurrence of roof failures in underground coal mines is a real matter of concern for mining engineers and researchers. Numerical modeling techniques are successfully used by several researchers by simulating rock mass condition for stability assessment of mine openings. The analysis becomes crucial in case of weak and fragile rock formation. The present research envelops the determination of 31 cases of rock load by CMRI-ISM RMR under different geo-mining conditions followed by the development of modified Rock Mass Rating (RMR), i.e., rock mass rating dynamic (RMR_{dyn}) by incorporating P-wave velocity as a new parameter. The rock load determined using RMR_{dyn} and numerical models was correlated and found in close agreement. In addition, the deviation in rock load determined by all the three approaches, i.e., CMRI-ISM RMR, numerical modeling, and RMR_{dyn}, was compared with the actual field data. The percentage deviation obtained in RMR_{dyn} and numerical modeling is less compared to CMRI-ISM RMR.

Keywords Rock load · Support design · Numerical modeling · CMRI-ISM RMR · RMR_{dyn}

1 Introduction

Roof fall takes place in the newly developed faces during mine development or depillaring owing to the resettlement of excavation-induced stresses. Roof fall is more vulnerable mainly for fragile rock formation encountered with more geological discontinuities. It leads to detrimental effects such as fatal or serious injuries to workers, stoppages in mining operations, and breakdown of equipment [1]. Most injury-causing roof falls involve falls of small chunks of roof rock from the immediate roof [2]. According to Ashish et al. (2016), 41% of accidents occur due to ground movement. The fall of the roof provides constructive information relating to the behavior of the immediate roof strata under specific geo-mining conditions. An investigation of roof falls reveals the principal causes of the roof fall and it is also of prime importance to establish or develop suitable support design based on the study of site-specific rock mass conditions [3]. Rock reinforcement using roof bolts has proved successful and is the principal support in underground development headings. The perception of the causes of roof failure is key in solving the problem of support-related issues. The complexity of geological disturbances and intricacy of the mining environment with respect to shale degradation, stress condition, and mining condition are some of the broad causative factors of roof failure in coal mines. Rock mass classification system and selection of appropriate type and capacity of support contribute to the decrease of roof fall in underground mines [4].

Rock mass classification systems, which are empirical in approach, are helping in the design of support system for underground mine openings and tunnels for more than a century now and are continuously evolving [5]. Thus, the limitations of such rock mass classification systems need to be understood properly for their application and design of a rational support system [6]. A rock mass classification

✉ Avinash Paul
avinashpaul@cimfr.nic.in

1 CSIR - Central Institute of Mining & Fuel Research, Dhanbad 826015, India

2 Department of Mining Engineering, Indian Institute of Technology (Indian School of Mines), Dhanbad 826004, India

system is a simple method to deal with complex rock mechanics problems in engineering design. Primarily, the system facilitates the estimation of rock mass properties like modulus of deformation and also provides proper support design guidelines and the stand-up time for underground entries [7]. The empirical approach helps in proper rock load estimation and in turn also increases the stability of the mine openings [8].

Application of the numerical modeling is a persuasive tool for the stability analysis of mines [9]. It is being widely used for the assessment and design of pillar stability as well as stability of underground mine openings with respect to in situ ground condition [10]. Both empirical and numerical approaches are implemented for stability analysis and support design for underground openings [11, 12]. Modelling and simulation with varied design inputs and geometry are viable methods for solving the complex geotechnical problems [13]. Intact and rock mass properties determined in field and laboratory data are required as input parameters used as stress, depth, RMR, cohesion, angle of internal friction, and tensile strength for numerical modelling. With the help of aforesaid input parameters, the failure zone (rock load height) is determined which helps design and selection of appropriate support for rock mass [14, 15]. Numerical modelling techniques were successfully used by several researchers for the simulation of the stability of mine openings in different geo-mining conditions ([11, 16–18]. The most important thing in numerical modelling is the selection of an appropriate method for simulation [19, 20]. Given the appropriate input parameters numerical modelling can predict the horizon of the roof failure which is also termed rock load height. In this paper, attempts were made to determine the rock load height using the Mohr-Coulomb model followed by validation from the empirically developed RMR$_{dyn}$ rock load predictor model. The propagation of rock failure can be more accurately predicted using the elastoplastic model (Mohr-Coulomb) compared to elastic models, and hence, this model was selected for the analysis. In this study, RMR$_{dyn}$ was developed, based on key limitations of the existing CMRI-ISM RMR system. Sonic velocity (P-wave velocity) of roof rocks was included as one of the parameters in the newly developed system with a perspective to involve geological variations to it.

2 Rock Mass Classification: a Review

Rock mass classification forms the backbone of the empirical design approach and is widely employed in rock engineering [14]. It has been experienced that when used correctly, a rock mass classification approach serves as a practical basis for the design of complex underground structures. The classification system in the last 50 years of its development has taken cognizance of the new advances in rock support technology starting from steel rib support to the latest supporting techniques like rock bolts and steel fiber reinforced shotcrete. The benefits and limitations of some of the well-known rock mass classifications are given in Table 1. After a detailed literature review, it was found that the presence of geological features like bedding planes, joints, and their orientation was the dominant parameter which affects rock stability during excavation. The research emphasis was placed on the CMRI-ISM RMR system as it was developed for Indian geo-mining conditions. However, the predominance of roof failure cases in spite of following the CMRI-ISM RMR system for support design is the key concern deserving a revisit.

Thus, the objective of the present research was based on the re-examination of the failed and stable roof cases for identification of the crucial parameters and in turn development of a modified rock mass classification by incorporating P-wave as rock mass rating dynamic (RMR$_{dyn}$) for addressing the roof failures.

2.1 Study Area

A total of 79 coal mine sites were investigated covering four major coalfields, i.e., Jharia Coalfield, IB Valley Coalfield (MCL), Godavari Valley Coalfield, and coalfields of South Eastern Coalfields Limited (SECL). Altogether, six coalfields of SECL were covered in the study namely Korba Coalfield, Sohagpur Coalfield, Bishrampur Coalfield, Chirimiri-Kurasia Coalfield, Jhilimili Coalfield, and Johilla Coalfield. Data were collected from the mine sites under varied geo-mining conditions to strengthen the objectives of the research work. Out of 79 investigated coal mine sites, thirty-one mine sites were selected, and twenty-nine mine sites were delineated where the roof condition was fragile and weak as the estimated RMR was categorized in poor roof condition with also a history of roof failure. The other two mine sites were selected from comparatively better roof condition to cover a wider RMR range. Thus, fragile/weak roof needs special attention while designing the support system because they are more vulnerable to roof fall causing injuries to the miners. The roof fall in such weak and fragile roof condition can take place because of the various reasons such as the presence of shear zone, slickenside, clay band, high horizontal stress, weak rock formation, and erroneous/faulty method of mining. Hence, safe mining under such roof condition becomes the key aspect for mine management by designing an appropriate and safe support system after a proper assessment of the roof condition. The study areas are demarcated in Fig. 1.
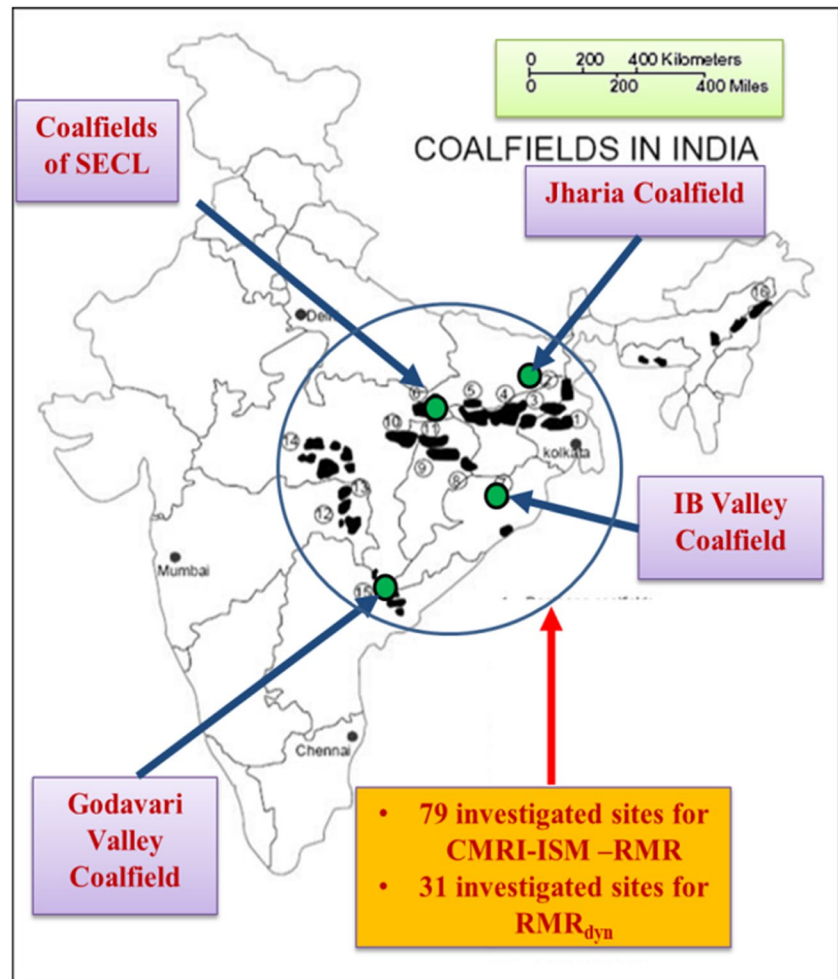
Table 1 Benefits and limitations of well-known rock mass classifications [21]

Name of classification	Author, year	Mathematical models	Benefits	Shortcomings
Rock quality designation (RQD)	Deere et al. [22] Priest and Hudson [23] Palmstrom [24]	$RQD = \frac{\sum (\text{core length} \geq 10\ cm)}{\text{Total length of core}} (x) 100$ $RQD = 115 - 3.3\ Jv$ $RQD = 100(0.1\lambda + 1)e^{-0.1\lambda}$	• Estimation is easy, hence–worldwide popular • RQD is good to account for fracture spacing • Used as very important parameter in various classification systems	• Does not reflect much about joint orientation. • Not suitable where rock mass consists of filling materials. • Not adequate to describe rock mass being a 2D representation.
Rock mass rating (RMR) Classification	Bieniawski [25]	Support load $(P) = \gamma \times B \frac{(100-RMR)}{100} = \gamma h_t$ Rock load height (h_t) $= B \frac{(100-RMR)}{100}$ B is the tunnel width (m), RMR is rock mass rating and γ is the density of the rock (kg/m³)	• Most popular and provides the basis for development of various classification systems • Used for design of support system in tunnels and mines	• Main emphasis is on joints rather than stresses, weathering and structural discontinuities. • Not suited for Indian condition as it shows 1 class deviation in the values.
Q classification system	Barton et al. [26]	$Q = \frac{RQD}{J_n} \times \frac{1}{J_r} \times \frac{J_w}{SRF}$ (Rock load) $P_{roof} = \frac{1}{J_r} \times \frac{1}{Q^{1/3}}$ (t/m²) (Rock load) $P_{roof} = \frac{2}{3} \frac{\sqrt{J_n}}{J_r} \times \frac{1}{Q^{1/3}}$ (t/m²)	Particularly suitable for highly jointed rock masses • Suitable for hard rock formations	• Not suitable for softer rock formation. • Parameters are based on joint attributes, whereas stability in coal mines is not only joint controlled. • Not applicable for multiple openings
Modified Rock Mass Rating system (MRMR)	Laubscher and Taylor [27] and Laubscher [28]	RMR = IRS + RQD + Spacing + Condition IRS=Intact rock strength, RQD=Rock Quality Designation, Spacing = Spacing of discontinuities, Condition = Condition of discontinuities MRMR = RMR* Adjustment factors	• It is a comprehensive and versatile system that has widespread acceptance by mining personnel • Used successfully in mathematical modeling	• Applicable only for caving
MBR (Final modified basic RMR)	Cummings et al. [29]	RMR=IRS+RQD+Spacing+Condition FMBR=AMBR x DC x PS x S DC=Distance to cave line PS=The block size adjustment S = The adjustment for orientation of major structures distance Adjusted MBR (AMBR) =MBR x A_b x A_s x A_o A_b= blasting adjustment A_s=stress adjustment A_o= fracture orientation adjustment	• Effect due to induced stresses, blasting and fracture orientation has been included which was not covered in the original RMR system	• Applicable for block cave mining. • Too many adjustment factors.
CMRI-ISM- RMR	Venkateswarlu et al.[30]	CMRI-ISM RMR = Layer thickness + Structural features + UCS + Slake durability +Ground water Rock Load (t/m²) = B*γ(1.7 - .037RMR + 0.0002 RMR^2), where, B= Roadway span (m) γ=Unit rock weight (t/m³)	• Most efficient classification system derived for Indian coal measure rock. • Easy and simple to apply. • Can be used up to 6m gallery width after applying adjustment factor.	• Stress adjustment is arbitrary in this system. • System applicable only for development workings. • Blasting adjustment given is arbitrary.

Table 1 (continued)

Name of classification	Author, year	Mathematical models	Benefits	Shortcomings
Critical Convergence & Rock Load	Ghosh and Ghosh [31]	Rock Load (t/m^2) = $\gamma \times 5B^{0.3}\left[\frac{100-RMR}{100}\right]^2$ Where, B = Roadway span (m) γ = Unit rock weight (t/m^3).	• For openings up to 5m for underground coal mines • Application is simple and easily adopted	• Not applicable for openings less than 5m in width. • Not applicable for the condition where concentration of stresses is more due to larger openings
Modified Q- System for Coal Mines	Sheorey [32]	Horizontal stratified rock -Changes J_n to $J_n^{2/3}$ Irregular bed thickness – Changes Q to Q/3 Ball coal in roof - Changes Q to Q/5 Stone/clay pockets - Changes Q to Q/3 Unfavorable joint orientation/ horizontal stress - Changes Q to Q/4 Rock Load $(P_{roof}) = K\gamma B(5Q)^{-0.33}$ (t/m^2)	• This classification is applicable for coal measure roof rocks • More adequate support design can be done for depillaring panels	• Not applicable for hard rock formation as it was modified for coal measure roof rocks • Although modification has been done, still this system has the shortcomings of Q system
CMRR (Coal Mine Roof Rating)	Molinda and Mark [33]	CMRR= UCS rating + Discontinuity intensity rating + Discontinuity shear strength rating + Multiple discontinuity adjustment + Moisture sensitivity deduction Support density ($ARBS_G$) = $(5.7\log_{10}H) - 0.35$ CMRR+6.5, Where, H =depth of cover	• Reliable and meaningful • Used in broad range of ground control issues • It quantifies the roof geology which helps extensively in mine planning.	• Estimation process is lengthy • System is relatively new hence all possible uses and specific guidelines not yet been determined • System is implemented in less mines and still lagging to develop data base to be accepted worldwide
Geological Strength Index (GSI)	Hoek [34]	GSI=RMR`$_{89}$ -5 for (GSI≥18 or RMR`$_{89}$≥23) GSI=9 ln Q` +44   Q`=(RQD/Jn).(Jr/Ja) GSI<18 RMR`$_{89}$ <23	• Qualitative and quick to use in field	• Applicable for both weak and hard rock masses • Used for computer simulation of rock masses • Experienced and expert persons can only use this system
Modified RMR System (RMR$_{Seis}$)	Murthy & Suresh [35]	Rock Load (t/m^2) = $0.0013RMR_{seis}^2 - 0.19RMR_{seis} + 9.25$	• Modified RMR incorporates the influence of blasting • Estimates the actual extent of damage zone in roof rocks due to blasting	• Less number of case studies, hence needs to be applied in varied conditions

Fig. 1 Map of India showing different coalfields covered in the study (After Dutta et al., 2011)

2.2 Basic Numerical Modeling Methods

The application of numerical modelling methods is commonly seen for solving various complex rock mechanics problems by converting them into simpler ones through discretization techniques. During this process, the total domain is discretized into smaller zones and meshes. Discretization is done, particularly, in the concerned area of stability assessment, for better evaluation of results. After the discretization model is defined with proper boundary conditions, different input rock properties are given according to the range defined. Horizontal and vertical stress values are also defined in the models with appropriate depth of the workings [36]. The main input parameters to be taken into account for analyzing the stability-related geotechnical problems are the geometry of the area, rock/rock mass properties (elastic modulus, strengths, RMR, etc. and in-situ stress field).

Some of the well-known numerical methods used for underground stability analysis are finite element method (FEM), finite difference method (FDM), boundary element method (BEM), distinct element method (DEM), discrete

fracture network (DFN) method, and hybrid models. In FEM, the whole area of the model is divided into a number of elements/meshes, and then respective rock properties are given with boundary conditions ([37]; Shivakumar and Maji, 2014). This technique is found suitable for solving the geomechanics problems related to the stability of any opening [38–40]. For FDM, the discretization of the study domain is done in the same manner as that of FEM [41–43]. This method is used for solving a wide range of problems by partial differential equations. This method can be applied to different boundary shapes with different materials for any region [44]. BEM needs very less computer memory for the storage of data as the boundary of the selected domain area is discretised or converted into smaller mesh. This method is applicable for three-dimensional analysis as it has a facility for the reduction in model size [45] and can be used for stability analysis of underground excavations. DEM is based on the principles of discontinuum mechanics [46, 47]. This method basically treats the zone of interest in the form of deformable rocks and is better suited for the study of a geotechnical problem [48] with geological discontinuities

efficiently. DFN method is useful for the application in fractured rock mass where the study of flow is to be analyzed [49] and where an equivalent continuum model is difficult to be established. This method has a capability to model the flow rate of liquid for fractured rock mass through simulation of packer tests [50, 51]. Hybrid models are generally applicable where the assessment of stress and deformation of the rock is a major concern. The main advantage of these models is that they take very less computing time for solving the complex geomechanics problems [52–54].

2.3 Numerical Modeling

2.3.1 Mohr-Coulomb Elastoplastic Model for Analysis

The Mohr-Coulomb criterion is based on elastoplastic analysis. In the elastoplastic analysis, the results are accurate and precise compared to the elastic analysis. Hence, to predict the propagation of rock failure accurately, the Mohr-Coulomb criterion was selected for the study. The Mohr-Coulomb model is most commonly used in the field of geotechnical engineering for analysis of rock behavior when subjected to stress. The analysis is based on the linear relationship between the normal and shear stress when applied to the intact rock samples. A linear relationship is generated by plotting the shear strength and applied normal stress, expressed as:

$$\tau = \sigma \ \tan \ (\Phi) + c \tag{1}$$

where τ is the shear strength, σ is the normal stress, c is the intercept on the shear strength axis, and Φ is the angle of internal friction. The basic concept of this model postulates that the failure takes place when the normal stress exceeds the shear strength of the rock. Material properties required as input parameters for Mohr-Coulomb elastoplastic model in numerical modeling using FLAC^{3D} are:

(i) Density of rock mass (t/m^3)
(ii) Bulk modulus (GPa) and
(iii) Shear modulus (GPa)

Instead of using Young's modulus of elasticity and Poisson's ratio directly, FLAC^{3D} uses bulk modulus and shear modulus. Both bulk modulus and shear modulus are evaluated using Young's modulus and Poisson's ratio by the following equations.

$$K = \frac{E}{3(1 - 2v)} \text{ GPa} \tag{2}$$

$$G = \frac{E}{2(1 + v)} \text{GPa} \tag{3}$$

where E is the Young's modulus in GPa, K is the Bulk modulus in GPa, G is the Shear modulus in GPa, and v is the Poisson's ratio.

The modeling was conducted in four stages as shown in Fig. 2.

Factors affecting the rock load height (extent of failure zone) are discussed below:
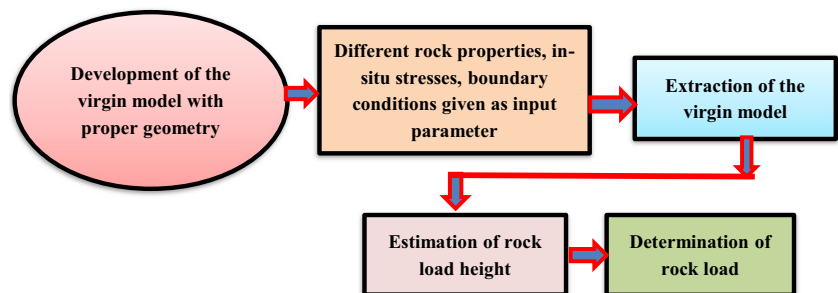
i) In Situ Stresses

The in situ stresses affect the stability of the underground mine openings. The idea of horizontal in situ stress condition is important for designing underground mining structures, especially during the development of a coal seam. The knowledge of in situ stress condition during the excavation is very important so that the support design for the excavated area is done accordingly. Sheorey [55] proposed an equation for the average in-seam horizontal stress which was based on a thermo-elastic shell model of the earth. He observed that the mean in situ horizontal stress (mean of the major and minor horizontal stresses) depends on the elastic constants (E, v), the coefficient of thermal expansion (β), and the geothermal gradient (G). This theory gives the value of mean horizontal stress as:

$$\sigma_h = \frac{v}{1 - v}\sigma_v + \frac{\beta E G}{1 - v}(H + 1000)\text{MPa} \tag{4}$$

where H is the depth cover in meters, σ_v is the vertical stress, and σ_h is the horizontal stress. Sheorey et al. [56] developed an equation that is in agreement with the existing stress measurement data from different parts of the world. This does not include actual measured data from Indian

Fig. 2 Sequential steps for estimation of rock load by numerical models

coalfields. In situ stresses were simulated with reference to Indian geo-mining condition.

The vertical in situ stress, induced due to gravity, was taken as:

$$\sigma_v = 0.025 \, H \, \text{MPa} \tag{5}$$

According to Sheorey [56], the values of different parameters of Eq. 4 for Indian coal measures are given as:

$$\nu = 0.25, \beta = 3 \times 10 - 5/°C, E = 2000 \, \text{MPa}, G = 0.03°C/m$$

After substituting the above values, the relation obtained for mean horizontal stress is expressed as:

$$\sigma_h = 2.4 + 0.01 \, H \, \text{MPa} \tag{6}$$

ii) Depth of Cover

Depth of cover affects the loading behavior of the overlying strata on the immediate mine roof. Generally, mining-induced stresses are high for greater depth of cover [57]. Thus, the depth of cover is considered one of the major factors for the estimation of rock load height in the numerical models. The depth of cover taken into consideration for different models varied from 45 to 400 m for rock load prediction. All these depth values were taken up to the roof of the seam.

iii) Boundary Conditions

Fine discretization was done for the roof rocks up to the height of 5 m for precise and accurate results for delineating the rock load height. The mesh size was kept uniform (0.25 m) on the roof of the roadway. The modelling of the roadways/galleries was done using a plane-strain model. The boundaries were kept sufficiently away from the excavation (minimum 50 m on all sides). Half of the roadway was modelled by applying a symmetric boundary condition using a vertical plane of symmetry passing through the center of the roadway. Fixed boundary conditions were used at the bottom. The side boundaries were restricted in lateral movement but kept free for vertical movement ("roller" boundaries). The surface was kept free. All modelling was done using the well-known software FLAC^{3D}, which computes in finite difference method [58]. The analysis of the results for roadway stability was done using Mohr-Coulomb elastoplastic analysis.

2.3.2 Experimental Procedure

i) Density

Vernier caliper is used to measure specimen dimensions to an accuracy of 0.1 mm. The mass of the sample is kept above 50 g as recommended by the ISRM [59] suggested method. The specimen bulk volume is calculated from an average of several caliper readings for each dimension. The specimen is dried to a constant mass at a temperature of 105°C, allowed to cool for 30 min in a desiccator, and its mass is determined. Density (γ) is calculated as the ratio of mass to volume.

ii) Uniaxial Compressive Strength

Uniaxial compressive strength, σ_c, is intended to measure the strength of a rock sample in uniaxial compression of a specimen of regular geometry. Test specimens are right circular cylinders having a height-to-diameter ratio of 2.5–3.0, and a diameter is kept approximately 54 mm. Load on the specimen is applied continuously at a constant stress rate such that failure will occur within 5 to 10 min of loading. The compressive strength of the specimen was determined using the following formula:

$$\sigma_c = \frac{F}{A} \tag{7}$$

where:

σ_c: uniaxial compressive strength (MPa)

F: load applied (N)

A: cross-sectional area of the specimen (mm^2)

The placement of the sample during uniaxial compressive strength determination is shown in Fig. 3.

iii) Tensile Strength

The specimen diameter is maintained at approximately 54 mm and the thickness is approximately equal to the specimen radius. Load on the specimen is applied continuously at a constant rate such that failure in the weakest zone of the specimen occurs within 15–30 s (Fig. 4). The tensile strength is arrived at using the following formula:

$$\sigma_t = 0.636 \, P/Dt \tag{8}$$

where:

σ_t: Brazilian tensile strength (MPa)
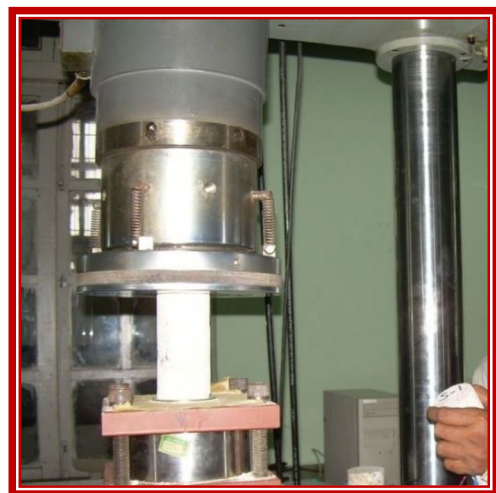
P: load at failure (N)
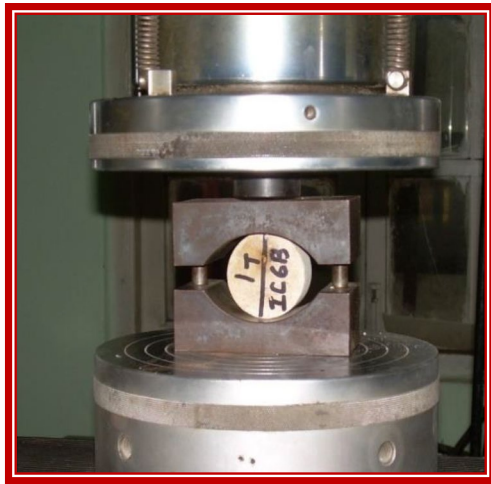

Fig. 3 Laboratory testing for σ_c test

Fig. 4 Laboratory testing for σ_t test

D: diameter of the specimen (mm)

t: thickness of the specimen (mm)

iv) Angle of Internal Friction (Φ) and Cohesion (c)

The strength value (UCS) is calculated by dividing the axial load (failure load) by cross-section of the area of the specimen. The obtained strength value is plotted against the corresponding confining pressure. The strength envelope is obtained by the best-fit straight line curve for the respective strength and confining pressure values as shown in Fig. 5. The point of *y*-axis intercept the (axial stress) is termed as "b," and the slope of the line is referred to as "m." The value of *b* and *m* is further used for the determination of cohesion (c) and angle of internal friction (Φ) from the following relationship:
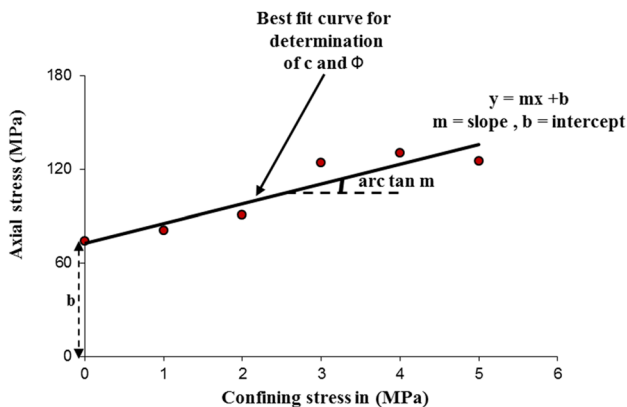
$$\Phi = \text{arc sin} \frac{m-1}{m+1} \tag{9}$$

$$C = b \frac{1 - \sin\Phi}{2\cos\Phi} \tag{10}$$

where:

Φ: angle of internal friction

C: cohesion

m: gradient of the line

b: intercepts of the *Y*-axis (axial stress)

v) Young's Modulus

Young's modulus, *E*, is measured at a stress level equal to 50% of the ultimate uniaxial compressive strength. The Young's modulus is measured using strain gauges mounted on a rock sample as shown in Fig. 6

The sample is loaded under a stiff testing machine (MTS). The data acquired by a data acquisition system (SPIDER 8) is analyzed using Catman software. The results are formulated in the form of a table. The Young's modulus is different for different rocks as the mineral composition and quartz content differ from one rock to another.

vii) Poisson's Ratio

Poisson's ratio, *v*, is calculated from the slope of the axial stress-strain curve and the slope of the diametric stress-strain curve (Fig. 7) and calculated using the following equation.

$$v = -\frac{\text{slope of axial stress} - \text{strain curve}}{\text{slope of diametric stress} - \text{strain curve}}$$
$$= -\frac{E}{\text{slope of diametric curve}}$$

Here, the slope of the diametric curve is calculated in the same manner as that for Young's modulus. Poisson's ratio in this equation has a positive value, since the slope of the diametric curve is negative.

2.3.3 Input Parameters

Proper estimation of strength and failure characteristics of rock mass is always required for any type of

Fig. 5 Strength envelope for determination of C and Φ

Fig. 6 Laboratory testing for determining Young's modulus

numerical simulation, whether it is related to support design or any other rock engineering design. Generally, Poisson's ratio values are in the range of 0.2 to 0.25 for all coal measure rocks, namely sandstone, shale, and coal. The least tested value of Poisson's ratio, i.e., 0.25, was taken considering the worst condition of the rock for coal and coal measure rocks, while the real values of remaining rock parameters were taken in modeling as listed in Tables 2 and 3.

2.3.4 Modeling Output

Rock load height (RLH) was determined for thirty-one mine sites by numerical modeling; a few of the models with varied gallery widths are shown in Figs. 8, 9, 10, 11, and 12. The roadway stability is depicted with respect to RHL and gallery width. The height of the shear and tensile zone, representing the gallery stability, determines RLH. Thus, the rock load is obtained by multiplying the RLH with the weighted density of the rock. Numerical modeling for the cases investigated considers the failure mode as both tensile and shear and the likely rock loads in such conditions.

2.4 Rock Load Estimation by Empirical Method

2.4.1 CMRI-ISM RMR

The stability of the roof is a function of several geo-mining factors such as geological anomalies, physicomechanical properties of rock, and stresses (virgin and induced). Based on a literature survey, detailed geotechnical studies, and statistical analysis, five major parameters were identified in CMRI-ISM RMR [60]. Each parameter was allocated a rating. The summation of individual parameter rating yields the rock mass rating (RMR). For simplicity, the minimum and

maximum values of RMR were taken as 0 and 100 respectively. The individual parameters and their maximum rating based on their influence on roof stability are provided in Table 4.

Weighted RMR is developed considering the number of rock layers in the roof up to a height of 2 m.

$$\text{Combined RMR}_w = \frac{\sum (\text{RMR of each bed X bed thickness})}{\sum (\text{Thickness of each bed})} \tag{11}$$

The adjustments for blasting and depth of working were applied for the RMR based on the geo-mining conditions. The adjusted RMR is then used for estimation of rock load in galleries and junctions from the following equations:

$$\text{Rock load in gallery } (\text{t/m}^2) = B \times D \times (1.7 - 0.037\,\text{RMR} + 0.0002\text{RMR}^2) \tag{12}$$

where RMR, rock mass rating; B, roadway width (m); and D, dry density (t/m^3).

Overall, from 79 investigated mine sites, 31 mine sites were selected, covering 29 mine sites with low RMR value and with roof fall cases, and two mine sites for stable cases.

2.4.2 Rock Load Estimation by RMR$_{dyn}$

A 3-channel handheld seismograph was used for P-wave determination for the minimum gallery width of 3.6 m without any difficulty. P-wave velocity is a proven technique to detect the layers of rock and to delineate the competence of rock mass. RMR$_{dyn}$ was determined for 31 mine sites considering four parameters, i.e., P-wave velocity, structural features, slake durability, and groundwater condition using a new rock mass rating system. UCS and layer thickness were replaced by P-wave velocity. Site-specific layer thickness determination is difficult in the underground mines if the strata are not exposed. Similarly, for UCS, the roof gets damaged due to the blasting of solid and affects the strength of the surrounding rock. If such rock samples are taken from the mine roof and tested for UCS, the actual representing value of compressive strength is not obtained. The P-wave velocity (also
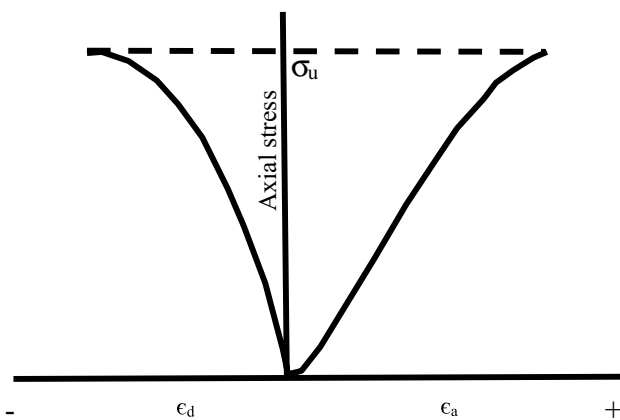

Fig. 7 Format of axial and diametric stress-strain curves

Table 2 Elastic constants taken for numerical simulation

Parameter	Rock type		
	Sandstone	Coal	Shale
Young's modulus (GPa)	5	2	2
Bulk modulus (GPa)	3.33	1.33	1.33
Shear modulus (GPa)	2.0	0.8	0.8
Poisson ratio, υ	0.25	0.25	0.25
Density (kg/m^3)	2500	1600	2500

Table 3 Input parameters taken for numerical simulation for intact rock

Sl. no.	Mine name	Depth (m)	RMR_{dyn}	σ_c (MPa)	Cohesion (MPa)	Φ (degree)	σ_t (MPa)
1	KTK 6 mine I seam II S.G Rise	190	40.5	7.25	0.406	32.21	0.69
2	KTK 6 mine I seam 13LN/BD	150	29.5	38.3	1.611	28.85	3.42
3	KTK 2 _ II Seam	180	46.2	8	0.443	33.93	0.6
4	KTK 6 mine II seam c dip/12LN	160	52.2	20	1.207	35.75	1.8
5	KTK 6 mine III seam main dip/3LS	140	61.67	21	1.455	38.58	1.9
6	VK Shaft King Seam	200	43	19.74	1.042	32.97	20
7	PVK 5 Shaft 6 King seam middle	312	40	20.27	1.022	32.06	1.98
8	JK 5 incline _35LS/39D	195	49	48.8	2.824	34.78	4.56
9	JK 5 incline _38LN/39D	188	45	35.3	1.919	33.57	3.2
10	Bartaria LK II Seam	45	45	7.23	0.391	33.57	0.7
11	Jamuna 1/2 Incline	100	40	18.71	0.943	32.06	1.65
12	Bhadra 7/8 incline	55	42	17.73	0.605	32.06	1.52
13	Jamuna 5/6 Incline	70	42	34.77	1.807	32.66	3.22
14	JhilimiliVseam	120	40	24.77	1.248	32.06	2.42
15	Bijuri	148	41	24.70	1.245	32.06	2.2
16	Kapildhara	35	48	30.4	1.727	34.48	2.96
17	Rajnagar RO	138	48	51.0	2.897	34.48	4.9
18	Haldibari	160	35	1.2	0.056	30.54	1.1
19	Pinoura	130	43.33	26.51	1.405	33.06	2.41
20	Nowrozabad	69	40	7.5	0.378	32.06	0.71
21	Piparia	90	35.67	15.37	0.722	30.74	1.34
22	Rehar mine	80	46.35	24.47	1.357	33.98	2.41
23	Vindhaya	95	38	9.84	0.480	31.45	0.85
24	Mine no 4 _24L/15DJ	70	45.33	35.49	1.939	33.67	3.22
25	Mine no 4 _34L/5D	103	45	23.3	1.267	33.57	2.1
26	Hirakhand bundia A′ section_ 76L/6D	93.93	49	29.2	1.689	34.78	2.78
27	Hirakhand bundia A section_76L/2D	88.83	51	30.8	1.827	35.38	3
28	Bhelatand XIII seam	400	37.8	17.6	0.857	31.39	1.54
29	Bhelatand XIV seam	330	39.6	24.2	1.212	31.94	2.32
30	15 Pit Sijua XII seam	290	39.48	18.25	0.913	31.91	1.76
31	8 Pit Sijua XII seam	347	40.5	25.94	1.317	32.21	2.31

Φ, angle on internal friction; σ_c, uniaxial compressive strength; σ_t, tensile strength

known as compressional wave velocity), a new parameter, replaced layer thickness and UCS in the present research. P-wave velocity was used to assess the extent of damage in the roof caused due to blasting-off-solid (BOS) in the underground mines and obtaining in situ rock mass condition. Hence, P-wave velocity was taken in the new model. The other parameters along with their respective rating remained the same as that of CMRI-ISM RMR. Thus, the new rating table for the determination of RMR_{dyn} is given in Table 5.

The maximum RMR_{dyn} of 61.67 (good roof condition) was found in KTK 6 mine, III seam main dip/3LS, and a minimum of 29.5 (poor roof condition) in KTK 6 mine, I seam 13LN/BD.

Rock load was determined using the following relation

$$RL \left(t/m^2\right) = B^* \gamma^* \left(31.85 RMR_{dyn}^{-0.79} - 1.14\right) \left(R^2 = 0.95\right)$$
(13)

where RL, rock load (t/m²); B, gallery width (m); and γ, rock density (t/m³).

A comparison of RMR determined by CMRI-ISM RMR and RMR_{dyn} for 31 mine sites is shown in Fig. 13.

3 Actual Rock Load Determination

The actual rock load was determined in 31 mine sites under varied geo-mining conditions. Roof fall patterns observed in the field were used as a benchmark for the estimation of rock load, shown in Fig. 14.
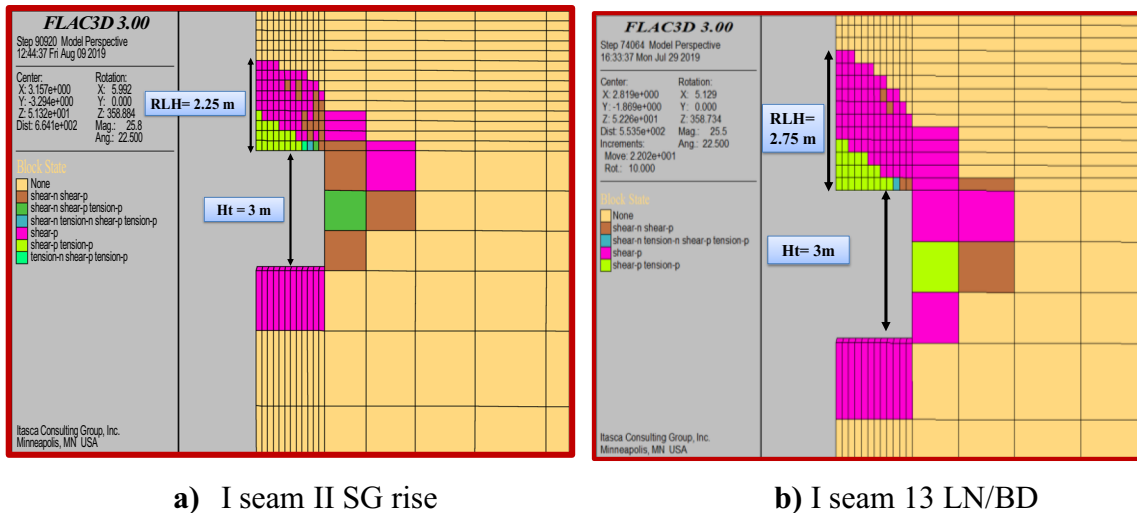
a) I seam II SG rise

b) I seam 13 LN/BD

Fig. 8 Modelled result showing yield zones for KTK 6 mine (gallery width 3.6 m)

a) PVK shaft 6 King seam middle section
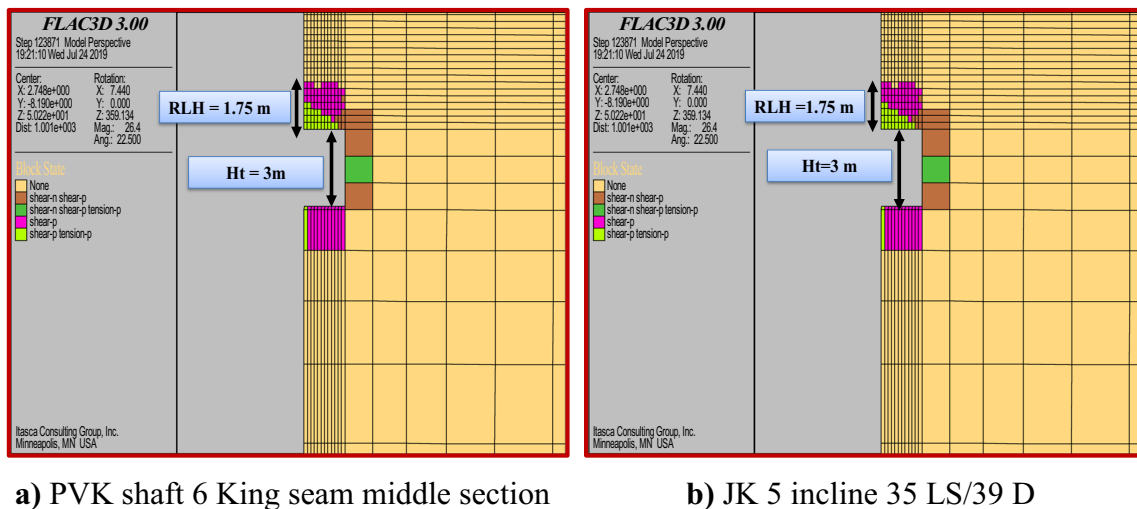
b) JK 5 incline 35 LS/39 D

Fig. 9 Modelled result for PVK shaft and JK 5 incline (gallery width 3.6 m and 4.2 m)

The different methods used for the estimation of rock load were roof fall height, exposed bolt length, and instrumentation using a load cell. The procedure for determination of rock load from roof fall height is obtained by multiplying the weighted density of roof rocks with the examined roof fall height. Similarly, the rock load estimated from exposed bolt length is the product of the measured exposed length and weighted density of roof rocks.

In general, for coal mine development galleries, 5–10 ton load cells are used, and in this research, the load-bearing capacity of the load cells used for the determination of rock load was 5 tons for improving the resolution of measurement and for precise roof monitoring. Vibrating wire load cells were installed at the center of the roof bolts in the development galleries for measuring the rock load. The load

is measured with the help of 3 to 6 vibrating wire sensors. The reading from individual sensors is averaged and used with a calibration factor given to the load cell to calculate the applied load. The rock loads estimated by different methods for actual field conditions are shown in Figure 15.

Rock load estimated from the field with different methods with stable and failed cases along with its roof bolt reaction is illustrated in Table 6.
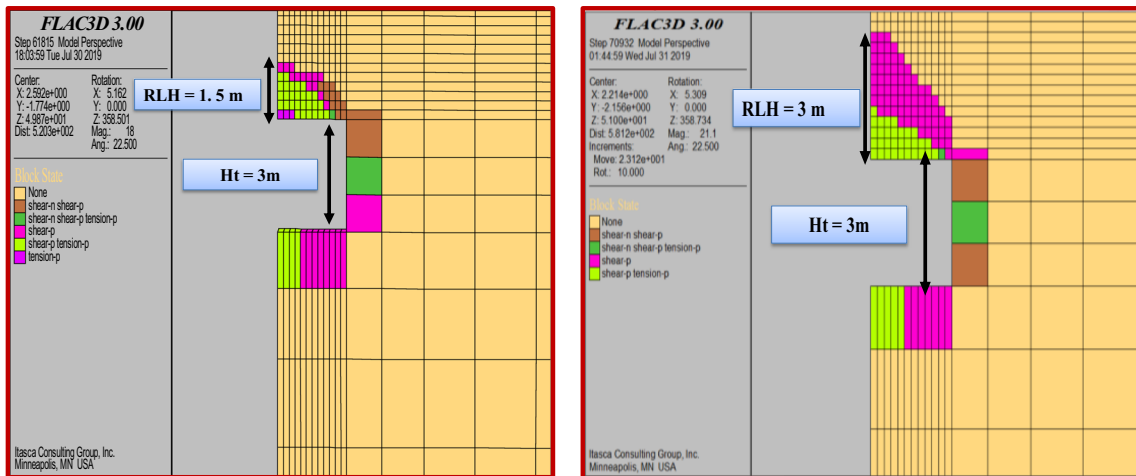
4 Validation

The rock load was determined for every site by multiplying the rock load height obtained from the model with the weighted density. The rock load obtained by the numerical
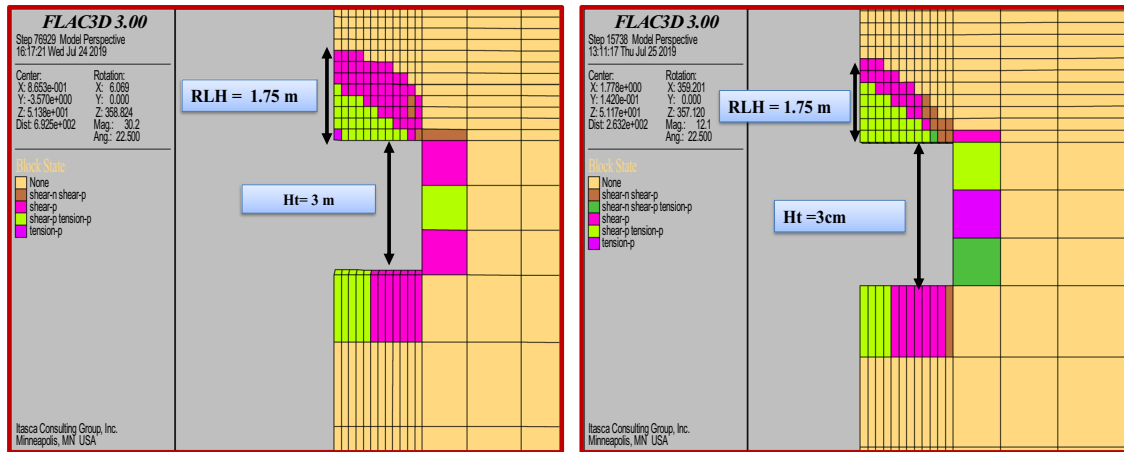
a) JK 5 incline 38 LN/39 D (gallery width 3.6m) **b)** Bartaria mine (4.2 m gallery width)
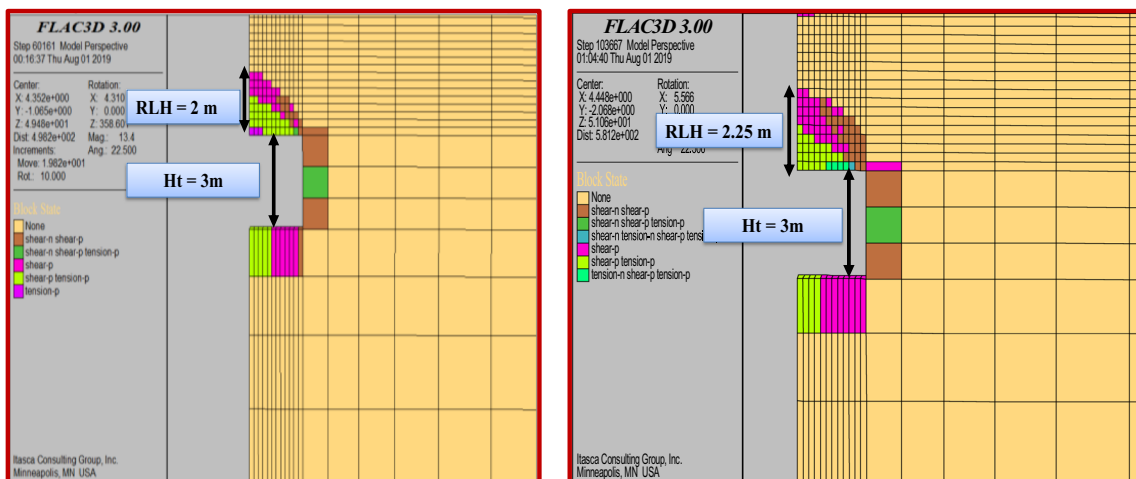
Fig. 10 Modelled result for JK 5 incline and Bartaria mine

a) Rajnagar RO mine **b)** Haldibari mine

Fig. 11 Modelled result for Rajanagar RO and Haldibari mine

a) Pinoura mine **b)** Nowrozabad mine

Fig. 12 Modelled result for Pinoura and Nowrozabad mine (4.5 m and 4.2 m gallery width)

Table 4 Maximum rating of parameters in CMRI-ISM RMR System (Venkateswarlu et al., 1987)

Parameters	Maximum rating
Layer thickness (cm)	30
Structural features (Structural Indices)	25
Weatherability (%) (1st Cycle slake durability index)	20
Rock strength (kg/cm^2) (Compressive strength)	15
Groundwater seepage rate (ml/min)	10

Table 5 Parameters of RMR$_{dyn}$ [21]

Parameter(s)	Maximum rating
P-wave velocity (m/sec)	45
Structural features	25
Weatherability (1st cycle slake durability index)	20
Groundwater condition (ml/min)	10

method was compared with the rock load estimated by RMR$_{dyn}$ as given in Table 7. A maximum standard deviation of 1.65 was observed. In most of the cases, a marginal deviation was observed.

A correlation between rock load estimated by numerical and empirical approaches is presented as shown in Fig. 16. Both are in close agreement with each other with a coefficient of correlation as 0.87 and an index of determination (R^2) as 0.77.

Rock load determined by numerical and empirical methods was validated with actual field data as shown in Figs. 17 and 18. The index of determination (R^2) for actual rock load and RMR$_{dyn}$ was observed as 0.94. However, in

the case of actual rock load and numerical approach, the index of determination (R^2) was estimated as 0.82.

The deviation in rock load from the actual was compared with all the three approaches, i.e., CMRI-ISM RMR, numerical modeling, and RMR$_{dyn}$ as shown in Fig. 19, and the corresponding average percentage deviation is shown in Fig. 20. A minimum percentage deviation of 7.19 % was obtained in the RMR$_{dyn}$ method.

Compared to other approaches, the correlation obtained between the actual rock load and RMR$_{dyn}$ is high (R^2 = 0.94) with a minimum percentage deviation of 7.19 %. Hence, RMR$_{dyn}$ can be used for rock load estimation for development galleries in underground coal mines under varied geo-mining conditions.

5 Results and Discussion

A critical review was done by comparing earlier rock mass classification systems. The review reveals that excavation technique, the presence of beddings and joints, and their orientation are the most dominant parameters causing instability of underground openings. Moreover, the adjustments proposed are repetitive in nature for some of the cases apart from being time-consuming. The main thrust was given to the CMRI-ISM RMR system as it was developed for Indian geo-mining conditions and is the suggested practice. The objective of the research comes into the limelight as there still exists a number of roof failure cases in spite of following the CMRI-ISM RMR system for support design. Thus, the present research aims at revisiting the failed and stable cases to identify the key parameters and attempt to develop a modified rock mass classification for addressing the roof failures.

Fig. 13 RMR determined by CMRI-ISM RMR and RMR$_{dyn}$ at different mine sites
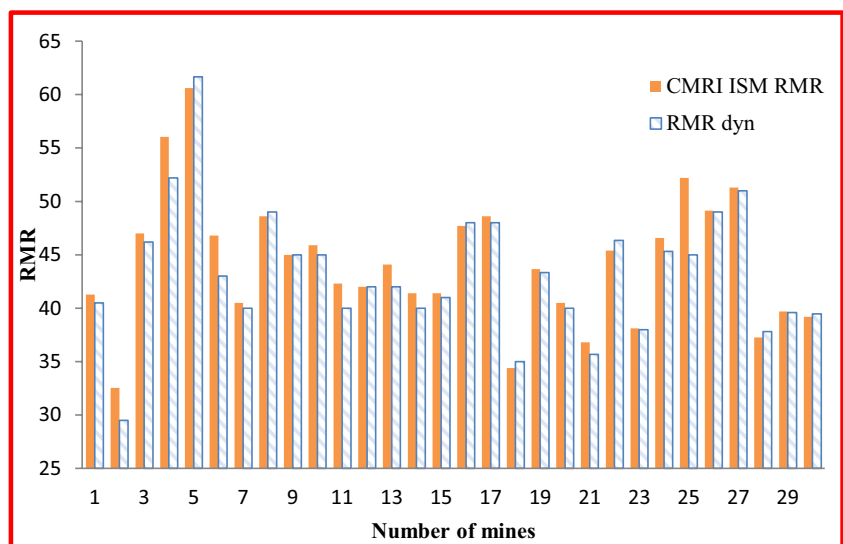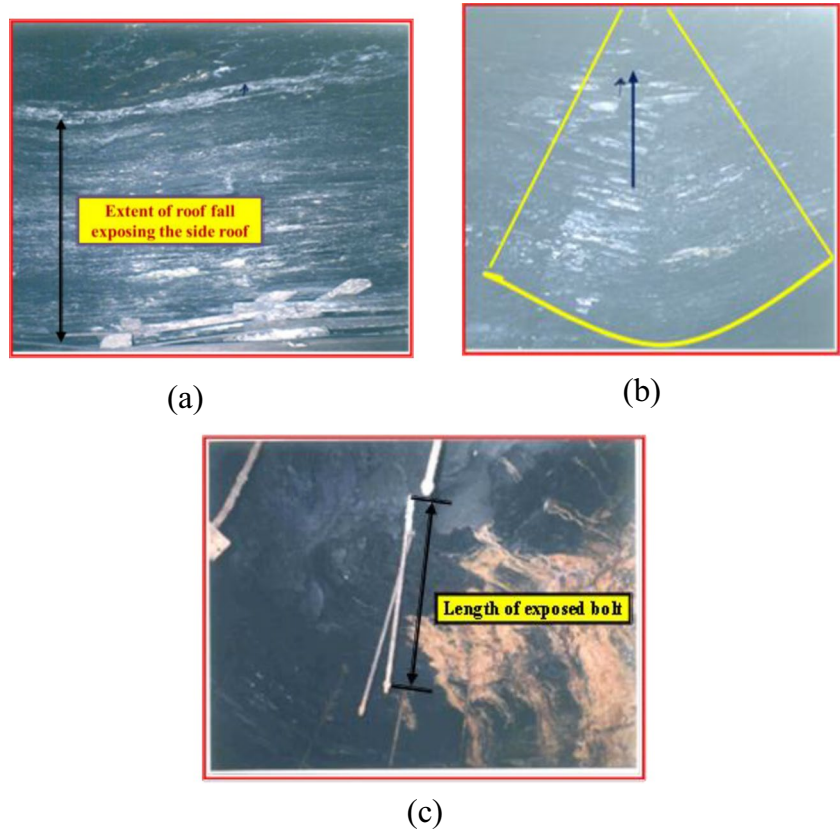
Fig. 14 Field observation of roof fall [21]. **a** Roof fall exposing the side roof, **b** loading arch with clear bending of coal seam, **c** exposed bolts due to detachment of layered beds

(a)

(b)

(c)

RMR was obtained for 31 mine sites by empirical method applying CMRI-ISM RMR system and RMR_{dyn}. The RMR estimated for CMRI-ISM RMR was found in the range of 29.27 to 60.62. Similarly, RMR_{dyn} recorded in 31 mine sites ranged from 29.5 to 61.67. The minimum and maximum value of RMR for both the approaches was found in the

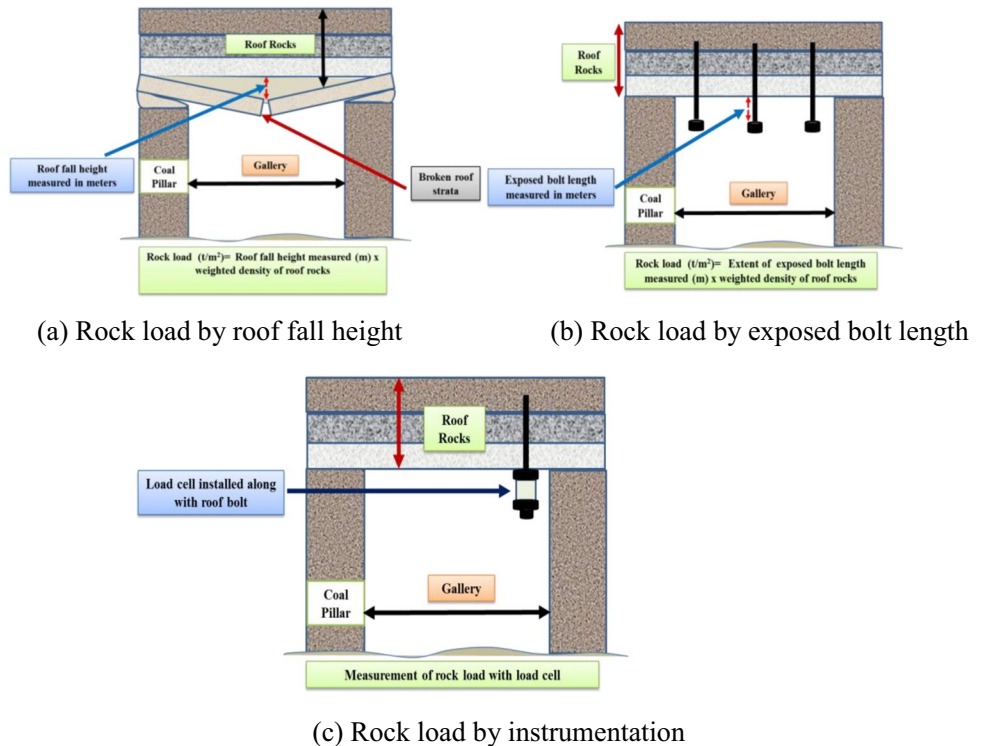**Fig. 15** Different methods of rock load determination in the field

(a) Rock load by roof fall height

(b) Rock load by exposed bolt length

(c) Rock load by instrumentation

Table 6 Rock load estimation by different approaches

Mine name	Actual rock load (t/m^2)	Rock load estimation method	Stable/failure	Applied roof support reaction
KTK 6 mine I seam II S.G Rise	4.57	RFH	Failed	Bolt failure resulting the roof failure up to 2.2 m
KTK 6 mine I seam 13LN/BD	6	RFH	Failed	Bolt failure resulting the rood failure up to 2.88 m
KTK 2 _ II Seam	3.45	RFH	Failed	Bolt failure resulting the roof failure up to 1.5 m
KTK 6 mine II seam c dip/12LN	2	Inst	Stable	Stable
KTK 6 mine III seam main dip/3LS	1.1	Inst	Stable	Stable
VK Shaft King Seam	4.7	RFH	Failed	Bolt failure resulting the roof failure up to 2.14 m
PVK 5 Shaft 6 King seam middle	4.28	RFH	Failed	Bolt failure resulting the failure up to 2.1m
JK 5 incline _35LS/39D	2.4	EBL	Failed	Roof fall exposing the bolt length up to 1.6 m
JK 5 incline _38LN/39D	2.55	EBL	Failed	Roof fall exposing the bolt length up to 1.7 m
Bartaria LK II Seam	3.85	RFH	Failed	Bolt failure resulting the roof failure up to 1.9 m
Jamuna 1/2 Incline	5.3	RFH	Failed	Bolt failure resulting the roof failure up to 2.49 m
Bhadra 7/8 incline	4.16	RFH	Failed	Bolt failure resulting the roof failure up to 2.31m
jamuna 5/6 Incline	4	RFH	Failed	Bolt failure resulting the roof failure up to 2.2 m
Jhilimili V seam	3.22	RFH	Failed	Bolt failure resulting the roof failure up to 2.3 m
Bijuri	4.9	RFH	Failed	Bolt failure resulting the roof failure up to 2.41
Kapildhara Mine	3.1	EBL	Failed	Roof fall exposing the bolt length up to 1.4
Rajnagar RO	3.2	EBL	Failed	Roof fall exposing the bolt length up to 1.4 m
Haldibari mines	5.68	RFH	Failed	Bolt failure resulting the roof failure up to 3.4 m
Pinoura mine	4.25	RFH	Failed	Bolt failure resulting the roof failure up to 2.5 m
Nowrozabad mine	5.22	RFH	Failed	Bolt failure resulting the roof failure up to 2.75 m
Piparia Mine	5.8	RFH	Failed	Bolt failure resulting the roof failure up to 3.2 m
Rehar mine	3.4	EBL	Failed	Roof fall exposing the bolt length up to 1.7 m
Vindhaya Mine	4.34	RFH	Failed	Bolt failure resulting the roof failure up to 2.68 m
Mine no 4 _ 24L/15D	2.62	EBL	Failed	Roof fall exposing the bolt length up to 1.6 m
Mine no 4 _ 34L/5D	3.29	EBL	Failed	Roof fall exposing the bolt length up to 1.7 m
Hirakhand Bundia A′ section	2.97	EBL	Failed	Roof fall exposing the bolt length up to 1.45 m
Hirakhand Bundia A section	1.83	EBL	Failed	Roof fall exposing the bolt length up to 1.18 m
Bhelatand mine XIII Seam	3.93	RFH	Failed	Bolt failure resulting the roof failure up to 3 m
Bhelatand mine XIV Seam	4.55	RFH	Failed	Bolt failure resulting the roof failure up to 2.6m
15 pit Sijua XII Seam	5.09	RFH	Failed	Bolt failure resulting the roof failure up to 2.8m
8 pit Sijua XII Seam	3.7	RFH	Failed	Bolt failure resulting the roof failure up to 2.5 m

RFH roof fall height, *EBL* exposed bolt length, *Inst* instrumentation

Godavari Valley Coalfields of Singareni Collieries Company Limited (SCCL). Few sites showed high RMR due to high compressive strength, greater P-wave, high slake durability, and less jointed rock mass with dry roof condition. On the other hand, low RMR values were due to less compressive strength and P-wave, highly weathered and jointed rock mass, and a watery roof condition with the occurrence of prominent slip.

After determining RMR, the rock load was obtained by applying empirical, numerical and actual field measurement. The variation in the rock load found for CMRI-ISM RMR system was scaled in the range of 1.5 t/m^2 to 5.90t/m^2. Similarly, for RMR$_{dyn}$, the range of rock load was noted between 0.77 and 8.06 t/m^2. Rock load was measured in the field by roof fall height, exposed bolt length, and instrumentation.

The rock load variation was observed between 1.1 and 6 t/m^2. For all the approaches, the maximum rock load values were found for KTK 6 mine I seam 13LN/BD and minimum rock load values for KTK6 mine III seam dip/3LS of Godavari Valley Coalfields (SCCL). The maximum and minimum values of estimated rock load were due to a variation in compressive strength, P-wave velocity, slake durability, presence of joints, and dry and wet roof conditions. Rock load determined by numerical modeling was found on the scale of 1.63 to 5.85 t/m^2. For numerical models, the maximum rock load values were found at Jamuna 1/2 Incline mine of South Eastern Coalfields Limited (SECL), and the minimum rock load value was at KTK6 mine III seam dip/3LS of Godavari Valley Coalfields (SCCL).

Table 7 Estimation of rock load height and rock load by numerical and empirical models

Mine name	Rock load height (m)	Density (t/m³)	Rock load by numerical model (t/m²)	Rock load by an empirical approach (t/m²)	Standard deviation
KTK 6 mine I seam II S.G Rise	2.25	2.08	4.68	4.39	0.21
KTK 6 mine I seam 13LN/BD	2.75	2.08	5.72	8.06	1.65
KTK 2 _ II Seam	2.25	2.3	5.175	3.44	1.22
KTK 6 mine II seam c dip/12LN	1	2.17	2.17	2.13	0.03
KTK 6 mine III seam dip/3LS	0.75	2.18	1.635	0.77	0.61
VK Shaft King Seam	2	2.2	4.4	4.68	0.20
PVK 5 Shaft 6 King seam middle	1.75	2.04	3.57	3.94	0.26
JK 5 incline _35LS/39D	1.75	1.5	2.625	2.17	0.32
JK 5 incline _38LN/39D	1.75	1.5	2.625	2.82	0.14
Bartaria LK II Seam	1.75	2.03	3.5525	3.82	0.19
Jamuna 1/2 Incline	2.75	2.13	5.8575	5.39	0.33
Bhadra 7/8 incline	2.25	1.8	4.05	4.06	0.01
Jamuna 5/6 Incline	2	1.82	3.64	3.91	0.19
JhilimiliV Seam	2.25	1.4	3.15	3.21	0.04
Bijuri	2.25	2.03	4.5675	4.k5	0.08
Kapildhara Mine	1.75	2.2	3.85	3.44	0.29
Rajnagar RO	1.5	2.29	3.435	3.55	0.08
Haldibari mines	3	1.67	5.01	6.39	0.98
Pinoura mine	2	1.7	3.4	3.80	0.28
Nowrozabad mine	2.25	1.9	4.275	4.81	0.38
Piparia Mine	2.25	1.81	4.0725	5.84	1.25
Rehar mine	1.75	2	3.5	3.46	0.03
Vindhaya Mine	2.5	1.62	4.05	4.59	0.38
Mine no 4 _ 24L/15D	1.75	1.64	2.87	3.02	0.11
Mine no 4 _ 34L/5D	1.75	1.94	3.395	3.65	0.18
Hirakhand Bundia A′ section	1.25	2.05	2.5625	2.97	0.29
Hirakhand Bundia A section	1.25	1.55	1.9375	1.94	0.01
Bhelatand mine XIII Seam	2.5	1.31	3.275	3.76	0.35
Bhelatand mine XIV Seam	2.5	1.75	4.375	4.53	0.11
15 pit Sijua XII Seam	2.5	1.82	4.55	4.75	0.14
8 pit Sijua XII Seam	2.5	1.48	3.7	3.64	0.04

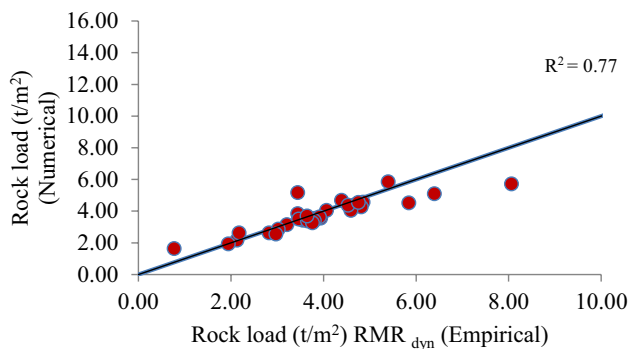Furthermore, the rock load obtained by numerical and empirical approach (RMR_{dyn}) was correlated. The coefficient of correlation of 0.87 and index of determination as 0.72 indicated a good relation. The study was further extended by comparing the deviation in rock load from all the three approaches (CMRI-ISM RMR, RMR_{dyn} and numerical
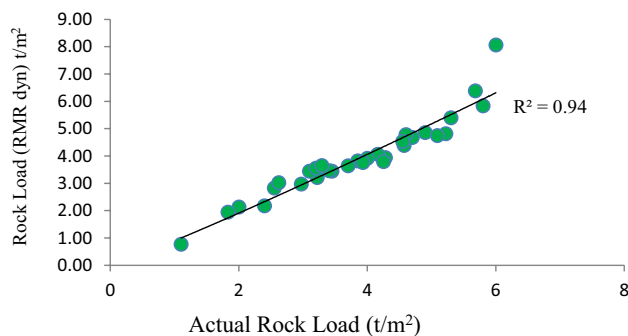
Fig. 16 Correlation of rock loads obtained by numerical and empirical approaches

Fig. 17 Correlation of actual rock loads and empirical approach (RMR_{dyn})
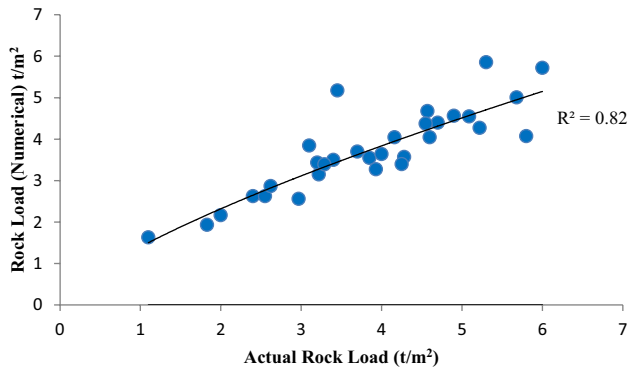
Fig. 18 Correlation of actual rock loads and numerical approach

Fig. 20 Percentage deviation of rock load by different approaches with actuals

modeling) with rock load obtained from actual field measurement. After comparing all the approaches, it was seen that the RMR_{dyn} showed a minimum deviation of 7.19%. Thus, statistical analysis and inter-relationship indicated that the newly developed rock load by RMR_{dyn} was reliable and significant in all means and hence can be used as a rock load predictor equation for the estimation of rock load for development galleries for underground mines.

6 Conclusions

RMR_{dyn} was determined in 31coal mine sites out of 79 investigated sites covering four coal fields, namely coalfields of South Eastern Coalfields Limited (SECL), Jharia Coalfield (BCCL and Tata Steel Limited), IB Valley Coalfield, and Godavari Valley Coalfield (SCCL). A critical review of the rock mass rating system in terms of its significance and function related to the application in Indian coal mines
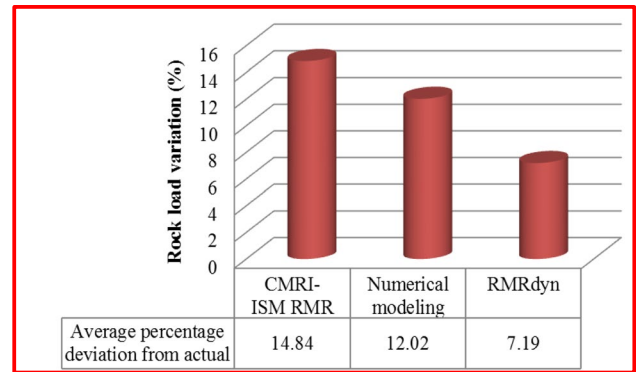
revealed that the presence of joints was the most dominant parameter for roof failure in underground mines.

In spite of the well-established CMRI-ISM RMR system for support design, still, the occurrence of a number of roof failure cases modified rock load predictor equation RMR_{dyn} was developed. RMR was determined for 31 mine sites applying CMRI-ISM RMR system and RMR_{dyn}. The RMR estimated for CMRI-ISM RMR was found in the range of 29.27 to 60.62. Similarly, RMR_{dyn} was on the scale of 29.5 to 61.67. The maximum RMR_{dyn} of 61.67 (good roof condition) was found in KTK 6 mine, III seam main dip/3LS, and a minimum of 29.5 (poor roof condition) in KTK 6 mine, I seam 13LN/BD.

The rock load found for the CMRI-ISM RMR system was scaled in the range of 1.5 to 5.90 t/m^2, and for RMR_{dyn}, the range of rock load varied between 0.77 and 8.06 t/m^2. The range of rock load found from actual field measurement was observed between 1.1 and 6 t/m^2.

Fig. 19 Deviation in rock load by different approaches with actuals
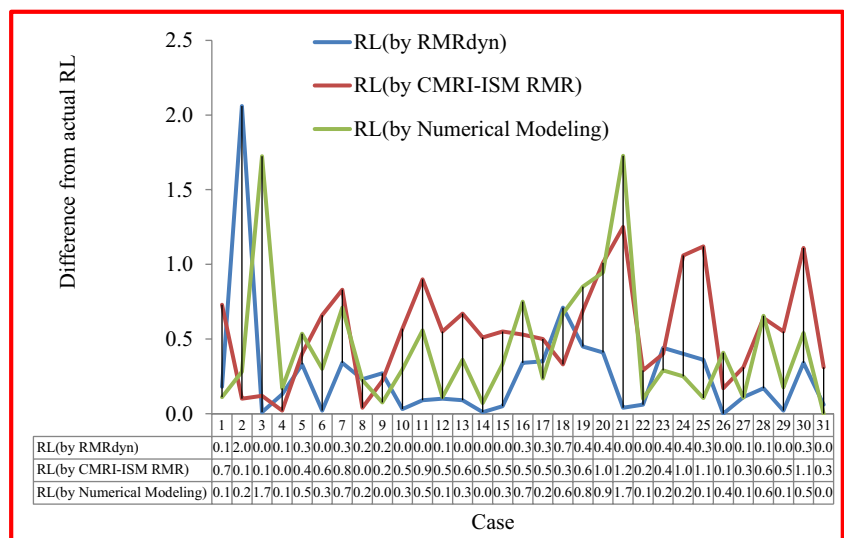
The propagation of rock failure can be more accurately predicted using the elastoplastic model (Mohr-Coulomb) compared to elastic models of numerical modeling, and hence, this model was selected in the analysis for the determination of rock load. The maximum and minimum rock load values obtained from numerical models were 5.85 t/m^2 and 1.63 t/m^2.

The rock load determined by empirical (RMR$_{dyn}$) and numerical methods was validated with actual rock load with a respective index of determination (R^2) of 0.94 and 0.82. The deviation of rock load of all the three approaches compared with actual field measurement showed minimum deviation in RMR$_{dyn}$ with 7.19%. Thus, it may be concluded that the derived new rock load predictor equation using RMR$_{dyn}$ is reliable and can be used for the estimation of rock load for development headings of underground coal mines.

Declarations

Competing Interests I hereby declare that there is no conflict of interests.

References

1. Kouros S, Kazem O, Ezzeddin B (2009) The 28th International conference on ground control in mining. Morgantown, West Virginia
2. Robertson S B, Hinshaw G E (2002) Roof screening, best practices and roof bolting machines. Proceedings of the 21st International conference on ground control in mining; Morgantown, WV, 189–194
3. Molinda G M (2003) Geologic hazards and roof stability in coal mines. Pittsburgh, PA: U.S. Department of Health and Human Services, Public Health Service, Centers for Disease Control and Prevention, National Institute for Occupational Safety and Health, DHHS (NIOSH) Publication No. 2003-152, IC 9466
4. Morissette P, Hadjigeorgiou J (2019) Ground support design for dynamic loading conditions: a quantitative data-driven approach based on rock burst case studies. J Rock Mech Geotech Eng 11(5):909–919
5. Ritter W (1879) Die static der tunnelgewolbe. Springer, Berlin
6. Palmstrom A, Broch E (2006) Use and misuse of rock mass classification systems with particular reference to the Q-system. Tunn Undergr Space Technol 21:575–593
7. Bieniawski ZT (1976) Rock mass classification in rock engineering. In: Bieniawski ZT (ed) Exploration for Rock Engineering, vol 1. Proc. of the Symp, Cape Town, Balkema, pp 97–106
8. Paul A, Murthy VMSR, Prakash A, Singh AK (2017) Performance investigation of rock mass classification systems for coal mine support design in Indian mining conditions. I. J. E. E. 10:1212–1219
9. Singh R, Kumar A, Singh AK, Coggan J, Ram S (2016) Rib/snook design in mechanised depillaring of rectangular/square pillars. Int J Rock Mech Min Sci 84:19–29
10. Sinha S, Walton G (2019) Numerical analyses of pillar behavior with variation in yield criterion, dilatancy, rock heterogeneity and length to width ratio. J Rock Mech Geotech Eng 11(1):46–60. https://doi.org/10.1016/j.jrmge.2018.07.003
11. Kushwaha A, Singh SK, Tewari S, Sinha A (2010a) Empirical approach for designing of support system in mechanized coal pillar extraction. Int J Rock Mech Min Sci 47:1063–1078
12. Shabanimashcool M, Li CC (2012) Numerical modelling of longwall mining and stability analysis of the gates in a coal mine. Int J Rock Mech Min Sci 51:24–34. https://doi.org/10.1016/j.ijrmms.2012.02.002
13. Basarir H, Oge IF, Aydin O (2015) Prediction of the stresses around main and tail gates during top coal caving by 3D numerical analysis. Int J Rock Mech Min Sci 76:88–97
14. Paul A, Singh AP, John LP, Singh AK, Khandelwal M (2012) Validation of RMR-based support design using roof bolts by numerical modeling for underground coal mine of Monnet Ispat, Raigarh, India—a case study. Arab J Geosci. https://doi.org/10.1007/s12517-011-0313-8
15. Ram S, Kumar R, Kumar A, Singh R, and Kumar D (2016). Numerical modelling based rock load height estimation at the goaf edge in a mechanised depillaring panel. Recent Advances in Rock Engineering (RARE 2016)
16. Verma A K, Deb D (2008) Numerical analysis of the interaction between hydraulic powered support and surrounding rock strata at Indian longwall faces. 12th International Conference of International Association for Computer Methods and Advances in Geomechanics (IACMAG), 1-6 October, 2008, Goa, India, 394-402
17. Yavuz H (2004) An estimation method for cover pressure re-establishment distance and pressure distribution in the goaf of longwall coal mines. Int J Rock Mech Min Sci 41:193–205
18. Zou DHS, Yu C, Xian X (1999) Dynamic nature of coal permeability ahead of a longwall face. Int J Rock Mech Min Sci 36:693–699
19. Hudson JA, Feng XT (2010) Technical auditing of rock mechanics modelling and rock engineering design. Int J Rock Mech Min Sci 47(6):877–886
20. Mercer RA, Bawden WF (2005) A statistical approach for the integrated analysis of mine induced seismicity and numerical stress estimates, a case study and evaluation of the relations - Part II. Int J Rock Mech Min Sci 42:73–94
21. Paul A (2020) Development of a rock mass classification (RMR$_{dyn}$) for rock load estimation in coal mine development headings of bord and pillar workings, Ph.D. thesis. IIT (Indian School of Mines), Dhanbad, Jharkhand, India, pp 1–201
22. Deere DU (1967) Technical description of rock cores for engineering purposes. Rock Mech Rock Eng 1:17–22
23. Priest SD, Hudson JA (1976) Discontinuity spacing in rock. Int J Rock Mech Min Sci Geomech Abstr 13:135–148
24. Palmstrom A (1982) The volumetric joint count – a useful and simple measure of the degree of the rock jointing, Proc.4th Congress, IAEG, Delhi, 5, 221-228.
25. Bieniawski ZT (1973) Engineering classification of jointed rock mass. Trans South Afr Civil Eng 15:335–344
26. Barton NR, Lien R, Lunde J (1974) Engineering classification of jointed rock mass for the design of tunnel support. Rock Mech 6:189–239
27. Laubscher DH, Taylor HW (1976) In: Bieniawski ZT (ed) The importance of geomechanics classification of jointed rock masses in mining operations, vol 1. Expl. for rock engg, Balkema, pp 119–128
28. Laubscher DH (1993) Planning mass mining operations. In: Hudson JA (ed) Comprehensive Rock Engineering, vol 2. Pergamon Press Oxford, New York, Seoul, Tokyo, pp 547–583

29. Cummings RA, Kendorski FS, Bieniawski ZT (1982) Caving rock mass classification and support estimation. U.S. Bureau of Mines Contract Report J0100103. Engineers International Inc, Chicago

30. Venkateswarlu V, Raju NM (1987) Support design for mine roadways - a geotechnical approach. In: World mining congress 13th. Stockholm, pp 857–864

31. Ghosh CN, Ghose AK (1992) Estimation of critical convergence and rock load in coal mine roadways – an approach based on rock mass rating. Geotech Geol Eng 10:185–202

32. Sheorey PR (1993) Experience with the application of modern rock classifications in coal mine roadways. In: Surface and Underground Project Case Histories. Pergamon Press, Oxford, New York, Seoul, Tokyo, pp 411–431

33. Molinda GM, Mark C (1996) Rating the strength of coal mine roof rocks. U.S. Department of the Interior, Bureau of Mines, Pittsburgh, PA

34. Hoek E, Marinos P, Benissi M (1998) Applicability of the geological strength index (GSI) classification for very weak and sheared rock masses. The case of the Athens schist formation. Bull Eng Geol Env 57:151–160

35. Murthy VMSR, Suresh R (2005) Seismic characterisation of coalmine roof for rock load assessment. First Indian Mineral Congress, Dhanbad, Jharkhand, India, pp 31–46

36. Singh UK, Singh GSP (2006) Numerical modeling of the caving behaviour of massive strata at a shallow depth longwall panel and dynamic loading effect. In: 1st Asian Mining Congress, The Mining Geological and Metallurgical Institute of India (MGMI), Centenary, 16-18 January, 2006. MGMI, Kolkata, India, pp 126–133

37. Loui JP, Sheorey PR (2001) Basics of numerical modeling. In: Proceedings, workshop theory and practice of ground control in bord and pillar mining. Central Mining Research Institute, Dhanbad, India, pp 35–39

38. Aksoy CO, Kantarci O, Ozacar V (2010) An example of estimating rock mass deformation around an underground opening using numerical modeling. Int J Rock Mech Min Sci 47:272–278

39. Jaiswal A, Shrivastva BK (2009) Numerical simulation of coal pillar strength. Int J Rock Mech Min Sci 46:779–788

40. Oraee K, Hosseini N (2007) Estimating coal pillar strength using finite element model, 1st International conference on mining and mining consequence, Mashhad, Iran, 2007

41. Mandal PK, Singh R, Maiti J, Singh AK, Kumar R, Sinha A (2008) Underpinning based simultaneous extraction of contiguous sections of a thick coal seam under weak and laminated parting. Int J Rock Mech Min Sci 45(1):11–28

42. Reddish DJ, Stace LR, Vanichkobchinda P, Whittles DN (2005) Numerical simulation of the dynamic impact breakage testing of rock. Int J Rock Mech Min Sci 42:167–176

43. Yasitli NE, Unver B (2005) 3-D numerical modeling of longwall with top coal caving. Int J Rock Mech Min Sci 42(2):219–235

44. Kumar A, Waclawik P, Singh R, Ram S, Korbel J (2019) Performance of coal pillar in deeper cover: field and simulation studies. Int J Rock Mech Min Sci 113:322–332

45. Kuriyama K, Mizuta Y, Mozumi H, Watanabe T (1995) Three dimensional elastic analysis by the boundary element method with analytical integrations over triangle leaf elements. Int J Rock Mech Min Sci, Geomech Abstract 32(1):77–83

46. Agliardi F, Crosta GB (2003) High resolution three-dimensional numerical modelling of rockfalls. Int J Rock Mech Min Sci 40(4):455–471

47. Xie Y, Zhao Y (2009) Numerical simulation of the top coal caving process using the discrete element method. Int J Rock Mech Min Sci 46:983–991

48. Sheorey PR, Murali Mohan G, Sinha A (2000) Influence of elastic constants on the horizontal in situ stresses. Int J Rock Mech Min Sci 38:1211–1216

49. Jing L, Stephenson O (2007) Discrete fracture network (DFN) method. Dev Geotech Eng 85:365–398

50. Lee HS, Son BK, Kim YG, Jeon SW (2006) Discrete fracture network and equivalent hydraulic conductivity for tunnel seepage analysis in rock mass. Tunn Undergr Space Technol 21:403

51. Xu C, Dowd P (2010) A new computer code for discrete fracture network modeling. Comput Geosci 36(3):292–301

52. Cai M (2008) Influence of intermediate principal stress on rock fracturing and strength near excavation boundaries-Insight from numerical modeling. Int J Rock Mech Min Sci 45:763–772

53. Coggan JS, Pine RJ, Styles TD, Stead D (2007) Application of hybrid finite/discrete element modelling for back-analysis of rock slope failure mechanisms. In: Proceedings of slope stability, International symposium on rock slope stability in open pit mining and civil Engineering, 12-14 September. pp 267–277

54. Jing L, Hudson JA (2002) Numerical methods in rock mechanics. Int J Rock Mech Min Sci 39:409–427

55. Sheorey PR (1994) A theory for in situ stresses in isotropic and transversely isotropic rock. Int J Rock Mech Min Sci Geomech Abst 31:23–34

56. Sheorey PR (2001) Design of pillars in underground coal mining. In: Course on theory and practices of ground control on board and pillar mining. CMRI, Dhanbad, Jharkhand, India, pp 91–115

57. Singh AK, Singh R, Maiti J, Kumar R, Mandal PK (2011) Assessment of mining induced stress development over coal pillars during depillaring. Int J Rock Mech Min Sci 48(5):805–818

58. Itasca (2012) FLAC3D (fast Lagrangian analysis of continua in 3 dimensions), version 3.0. Itasca Consulting Group Inc., Minneapolis, Minnesota, 55401, USA

59. ISRM (1977) Suggested methods for determining sound velocity, March.

60. Venkateswarlu V, Ghosh AK, Raju NM (1989) Rock-mass classification for design of roof support- a statistical evaluation of parameters. Eng Geol 8:97–107